New chromium steel grade for creep applications

Materials Research Express

PAPER

New chromium steel grade for creep applications

Lorena M Callejo[1,*], **José Ignacio Barbero**[1], **Mónica Serna-Ruiz**[1], **David Eguizabal**[1], **Roberto Fernandez Martinez**[2,*], **Pello Jimbert**[2], **Beatriz Calleja-Saenz**[3,*] **and Alejandra López**[3]

[1] TECNALIA, Basque Research and Technology Alliance (BRTA), Astondo Bidea, Derio, 48160, Bizkaia, Spain
[2] College of Engineering in Bilbao, University of the Basque Country UPV/EHU, Plaza Ingeniero Torres Quevedo 1, Bilbao, 48013, Bizkaia, Spain
[3] Tubacex Innovation, Ibaizabal Bidea, Derio, 48160, Bizkaia, Spain
[*] Authors to whom any correspondence should be addressed.

E-mail: lorenam.callejo@tecnalia.com, roberto.fernandezm@ehu.eus and bcalleja@tubacex.com

Keywords: martensitic steel, thermal treatment, creep behaviour

OPEN ACCESS

RECEIVED
23 August 2022

REVISED
20 September 2022

ACCEPTED FOR PUBLICATION
27 September 2022

PUBLISHED
11 October 2022

Abstract

In this study, a novel Chromium steel grade (COIN2) is produced as a result of a new steel composition and an innovative heat treatment. This new steel grade COIN2 evolves from the P92 steel grade and other novel steel grade recently created by the authors (COIN), and represents an enhancement of hardness, tensile properties, and creep behaviour with respect to them, which validates the metallurgical strategy used for further research in order to increase the efficiency of power plants and thus reduce the CO_2 emissions. The characterization reveals a significant property improvement with the innovative thermal treatment, contributing to the production of a novel and more competitive steel grade for creep applications.

1. Introduction

High Chromium martensitic steels [1–7] are excellent grades for high temperature applications due to their good corrosion properties and creep behaviour, thus being useful in power plants [8, 9]. Nevertheless, current demands to tackle climate change go towards more efficient electricity generation plants, for which new alternatives such as more competitive novel steel grades are required. In particular, high Chromium steel grades with improved behaviour in terms of creep resistance and corrosion properties could allow using steam pressures and temperatures above those used in current USC plants, which would contribute to more efficient power generation plants, resulting in reduced CO_2 emissions [10].

Extensive research has been devoted to the design and development of new grades for high temperature applications [11], such as P91 steel grade [12–14], which has been studied under different thermal treatments to analyse the precipitated phases and their influence on the mechanical properties. In the same context, and with the aim of further improving the creep resistance, P92 steel grade is developed [15, 16] and investigated through the application of different thermal routes. Other efforts to increase the corrosion resistance in creep steels led to the development of grades with higher Chromium content [17]. However, this strategy resulted in a decrease of the creep strength. P91 and P92 grades have demonstrated to be good candidates for creep applications at temperatures up to 620 °C.

In the present work, novel steel grades with a creep behaviour at 650 °C beyond that offered by the P92 grade are investigated for more efficient power generation. As a result of this investigation, a new 9Cr ferritic/martensitic steel [18, 19] is reported here, which has been produced from P92 by means of novel alloying [20–24] combined with an innovative heat treatment [25–28]. In comparison to previous P92 modified steels, the new grade here presented (COIN2) offers improved creep behaviour and other mechanical properties that potentially allow operating in more demanding conditions in terms of temperature and pressure for more efficient power generation (reduced CO_2 emissions). These properties are given by the steel microstructure, which is controlled through the metallurgical strategies here applied [29–31].

Figure 1. Type of ingots cast at lab scale, type of bars forged from the ingots (dilatometry samples and cylinders treated and investigated were cut from the forged bars), furnace and salt bath installation used in the lab scale heat treatments.

2. Materials and methods

The innovative composition and thermal treatment of COIN2 were selected according to bibliography, the commercial software JMatPro (British Thermotech), and studies on a LINSEIS L78 RITA dilatometer, pursuing the microstructural control and the mechanical improvement. In particular, the critical temperatures for phase transformations (Ac1, Ac3, Ms, Mf) were obtained by means of a LINSEIS L78 RITA dilatometer using cylindrical samples 3 mm in diameter and 10 mm in length, by applying the tangent method to the normalizing curve. With this information, martensite transformation curves could be calculated. Therefore, quenching temperatures for the martensitization step that correspond to 10% and 30% of untransformed austenite (MT10 and MT30) could be also determined. The heating rate applied was 5 °C s^{-1} for normalizing, and 15 °C s^{-1} for tempering; the cooling rate applied was 20 °C s^{-1}; the dilatometry experiments were carried out in Helium atmosphere. The holding time for normalizing as well as for martensitization step was 4 min, keeping a holding time of 8 min for tempering.

An induction furnace (INDUCTOTHERM VIP POWER TRACK 50 kW) with a capacity of 30 Kg was employed for ingot casting in air. Once the lab scale ingot had been forged, muffle furnaces and a salt bath installation were used to apply the thermal treatments on lab scale cylinders (figure 1).

Infrared absorption (LECO® CS 400 Carbon/Sulfur Determinator) and plasma emission spectrometry (Varian Vista MPX simultaneous Induced Coupled Plasma Optical Emission Spectrometry analyser) were used for the chemical analysis of the composition. The microstructure of the steel samples was analysed by optical microscopy (LEICA microscope), and Environmental Field Emission Scanning Electron Microscopy coupled with Energy Dispersive x ray spectroscopy (FESEM EDX). Grain structure of the samples was revealed by a 3% Nital solution. The structure of the samples was investigated by x-ray diffraction (XRD) measurements taken at room temperature on a X'Pert diffractometer (Cu Kα radiation) and analysed by X'Pert HighScore software.

The tensile properties were measured at room temperature with a tensile test equipment (INSTRON 5501). A FV 700 FUTURETECH Vickers Hardness Tester was utilized for the determination of the hardness values. The creep resistance was analysed using a creep test machine (in-house IPM designed) (load capacity of 8 kN between 150 °C–950 °C): the tests were done in constant load regime in Ar; the specimen elongation was recorded and the strain rate was calculated by test monitoring software; specimen dimensions = 6 mm in diameter, gauge length = 35 mm.

3. Results

3.1. Experimental procedure

The novel steel grade COIN2 was fabricated at lab scale to be compared to P92 and COIN steel grades previously produced by the authors at the same scale [32]. COIN2 experimental steel grade was fabricated by remelting the commercial steel P92 and adjusting its composition. After casting, the COIN2 steel grade was subjected to forging and heat treating through to 2 thermal treatments: the standard thermal treatment of the P92 commercial steel grade (TT1) and the innovative thermal treatment (TT2). This way, two different grades were produced for characterization: COIN2-TT1; COIN2-TT2.

Table 1. Composition (wt.%) of the COIN2 experimental steel grade (as cast steel sample).

Element	'COIN2' experimental steel grade
C	0.08–0.12
Mn	0.35–0.60
P, max.	0.020
S, max.	0.010
Si, max.	0.35–0.45
Cr	8–8.5
W	2.5–3.5
Co	2–2.5
Ni, max.	0.15–0.25
V	0.15–0.20
Nb	0.04–0.06
Ta	0.04–0.09
Nd	0.010–0.060
B	0.006–0.010
Al, max.	0.02
N	0.03–0.04
Mo	0.55–0.80
Ti, max.	0.01
Zr, max.	0.01
Ce	0.03–0.07

Table 2. Critical temperatures (°C) for the COIN2 experimental steel grade.

Steel grade	Ac1	Ac3	Ms	Mf	MT10	MT30
COIN2	827.9	982.3	402.8	233.6	301	337

3.2. Chemical analysis

The composition of the novel steel grade produced matches the one pursued with JMatPro and literature studies (table 1). In table 1, the chemical composition of the experimental steel grade COIN2 is shown.

3.3. Thermal treatments investigation

In order to design the thermal treatments to apply on the COIN2 experimental steel grade, previous investigations on this material were carried out through dilatometry.

The standard thermal treatment (TT1) is based on a normalizing treatment (1060 °C) followed by tempering.

On the other hand, the innovative thermal treatment (TT2) to be applied on COIN2 increases the normalizing temperature approximately 100 °C, reduces the tempering temperature 15 °C, and adds a martensitization step (intermediate step between normalizing and tempering where the steel after normalizing is cooled down to a temperature below Ms and above RT to retain a certain percentage of austenite). Such a novel processing route pursues an enhanced control of the microstructure [29].

Two percentages of retained austenite were selected to be obtained and explored: 10% and 30%. Therefore, two martensitization temperatures (MT) were chosen for COIN2 experimental steel to retain 10% (MT10) and 30% (MT30) of austenite, respectively.

The critical temperatures: Ac1, Ac3, Ms, and Mf of COIN2, together with the temperature for which a 10% of austenite is retained for this grade (MT10), and the temperature for which a 30% of austenite is retained for this grade (MT30), were determined from the dilatometry curve obtained when normalizing the COIN2 steel grade at 1060 °C. In table 2, the values obtained have been collected.

Accordingly, dilatometry samples of COIN2 were subjected to the innovative treatment (TT2) in two ways: (i) involving a martensitization at 301 °C (MT10), and (ii) involving a martensitization at 337 °C (MT30), (figure 3). The microstructure (figure 4) and hardness properties of the samples obtained (COIN2-TT2–301, COIN2-TT2–337) were studied in order to select the MT that offers best properties and treat this experimental steel grade accordingly at higher scale. The standard process was also applied to dilatometry samples of this grade (COIN2-TT1), which were conveniently characterised for comparison.

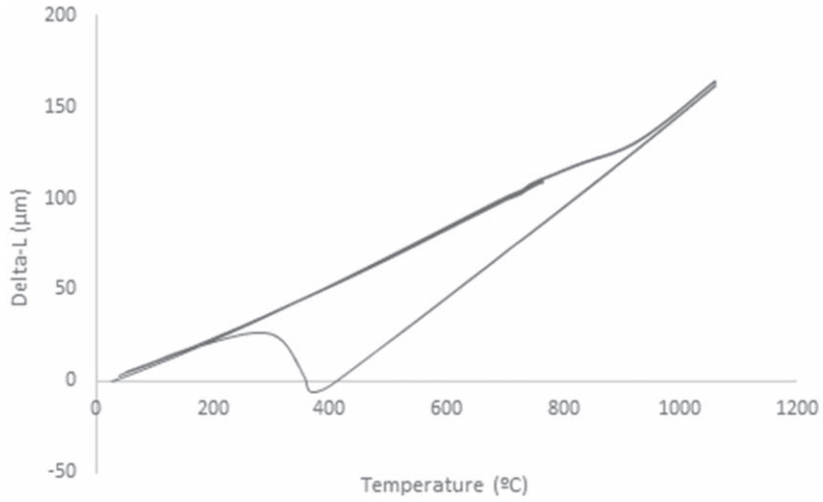

Figure 2. Dilatometry profile of COIN2-TT1: Normalizing involving a primary transformation (austenite to martensite), followed by tempering.

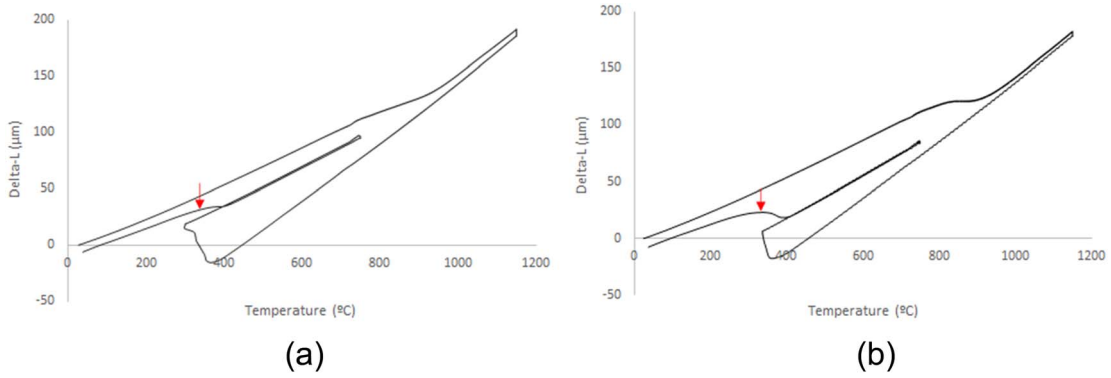

Figure 3. Dilatometry curves of COIN2-TT2–301 (a) and COIN2-TT2–337 (b). The more and less abrupt secondary transformations due to the martensitization can be observed.

After the application of TT1, tempered martensite is usually obtained (figure 2), since the composition of the steel grade potentially provides enough hardenability to facilitate the formation of martensite after normalizing without the necessity of applying too rapid cooling, and such martensite is then tempered.

With TT2, other options may arise. Based on literature [29], in the martensitization, the transformation of austenite into martensite is interrupted at certain temperatures (MT10 or MT30) at which some austenite (10% or 30%) can be retained and stabilized with the martensite formed. Afterwards, in tempering, that austenite may transform into ferrite and carbides/carbonitrides, and martensite is tempered. Even so, Santella *et al* [30] affirm that previously retained austenite is stable when tempering, giving fresh martensite in the final air cooling, which then coexists with the tempered martensite, thus increasing the steel hardness. Considering dilatometry profiles (figures 2 and 3), a primary transformation is experimented by the austenite obtained in normalizing, giving martensite (TT1) and some retained austenite (TT2). The latter is stabilized in the martensitization, experimenting a secondary transformation on cooling after tempering (figure 3). CCT curves suggest austenite transforms into ferrite at 800 °C, and into martensite at 400 °C. As this secondary transformation occurs at 400 °C, it confirms the possibility of the formation of fresh martensite from the austenite previously retained and stabilized [30, 33, 34]. The fresh martensite mentioned would coexist with the tempered martensite originally obtained in the primary transformation [30].

Comparing the dilatometry curves of COIN2-TT2–301 and COIN2-TT2–337, a more pronounced secondary transformation can be observed for a more elevated MT, because higher MT induces a higher amount of austenite retained and secondarily transformed (figure 3).

In thermal treatments TT2–301 and TT2–337 (figure 3), the primary transformation after normalizing (austenite to martensite) is stopped at MT10 (301 °C) to retain 10% of austenite and at MT30 (337 °C) to retain

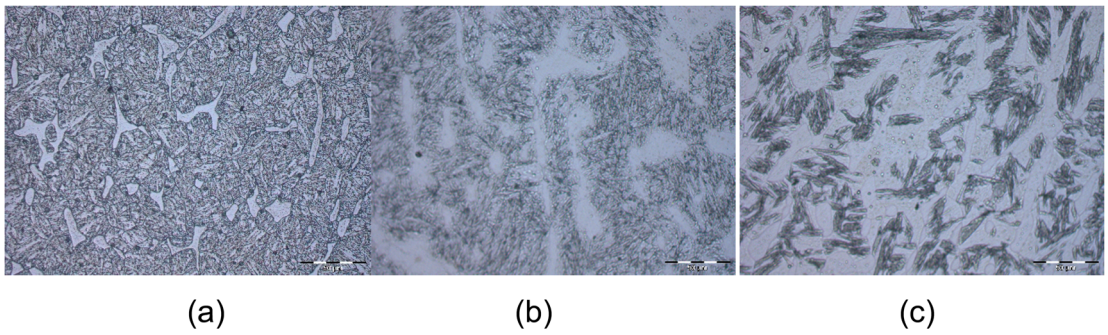

Figure 4. Microstructure of the COIN2 dilatometry samples after thermal treatment (Nital etching): COIN2-TT1 (a); COIN2-TT2–301 (b); COIN2-TT2–337 (c).

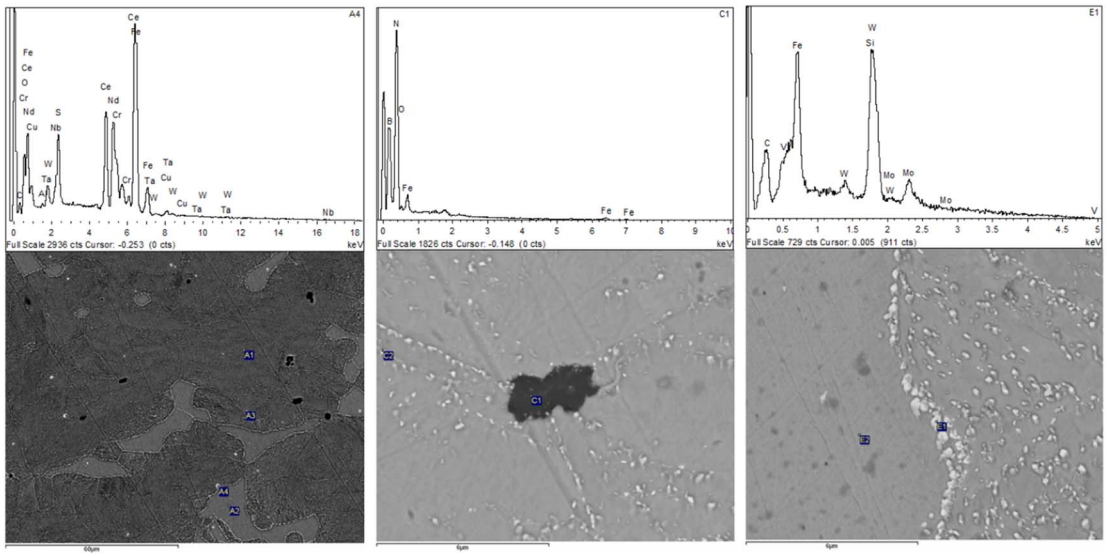

Figure 5. Phases and precipitates observed by FESEM EDX after TT1 (dilatometry sample: COIN2-TT1).

30% of austenite, which, after tempering, experiment a secondary transformation at 400 °C (indicated in red). The secondary transformation can be appreciated better if a higher percentage of retained austenite is transformed, and is given after the tempering of the martensite obtained in the primary transformation.

As expected, in TT1 (figure 4), tempered martensite is observed (in dark colour). However, clear islands of ferrite appear throughout the microstructure, maybe due to insufficient hardenability of the steel grade or a cooling rate after normalizing lower than necessary for a fully martensitic microstructure.

As it can be seen in figure 4, for higher MT (337 °C versus 301 °C), more austenite is retained and transformed at the end of the thermal treatment. The result of this secondary transformation appears in clear colour and could correspond to fresh martensite [30]. In addition, the possibility of ferrite formation after normalizing (as in TT1) or during tempering (from the austenite retained and stabilized, according to Tamura *et al* [29]) cannot be disregarded. More retained austenite also implies a lower concentration of martensite formed after normalizing and subsequently tempered (in dark colour). This type of martensite exhibits a more chaotic arrangement and laths of larger size for samples of higher MT.

The dilatometry samples COIN2-TT1 and COIN2-TT2–337 were studied by FESEM EDX in order to qualitatively analyse the different phases and the content of precipitates found in TT1 and TT2. After applying the standard thermal treatment TT1 (figure 5, left image), dark tempered martensite together with clear ferrite islands can be observed. After the innovative thermal treatment TT2–337 (figure 6, left image), two different types of martensite can be distinguished (fresh martensite in clear colour, and tempered martensite in dark colour) [35]. Moreover, micro and nanoprecipitates containing elements such as Ce, Nd, and Nb, or B and N, as well as containing W and Mo can be observed (figures 5 and 6).

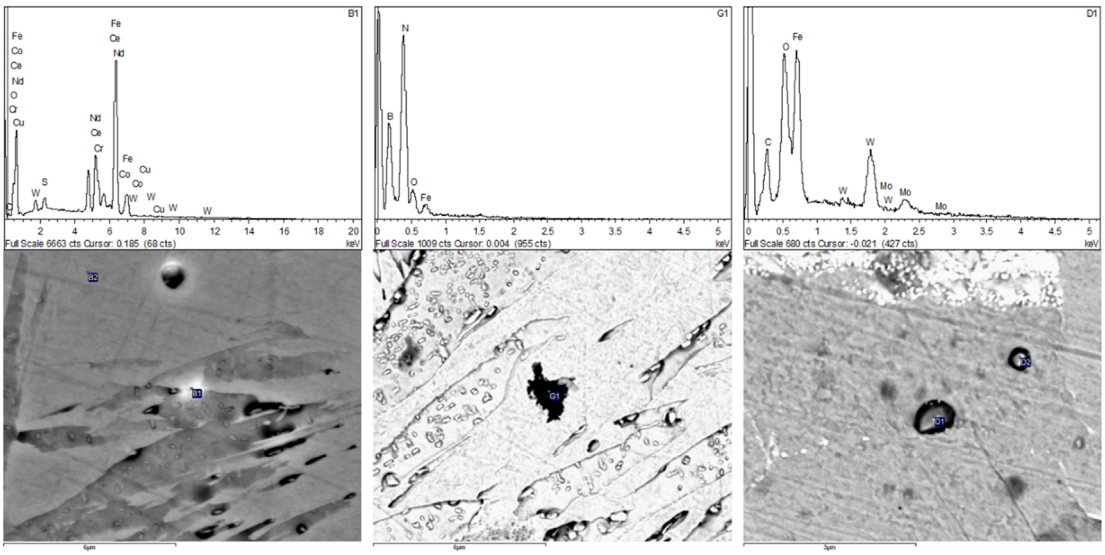

Figure 6. Phases and precipitates observed by FESEM EDX after TT2–337 (dilatometry sample: COIN2-TT2–337).

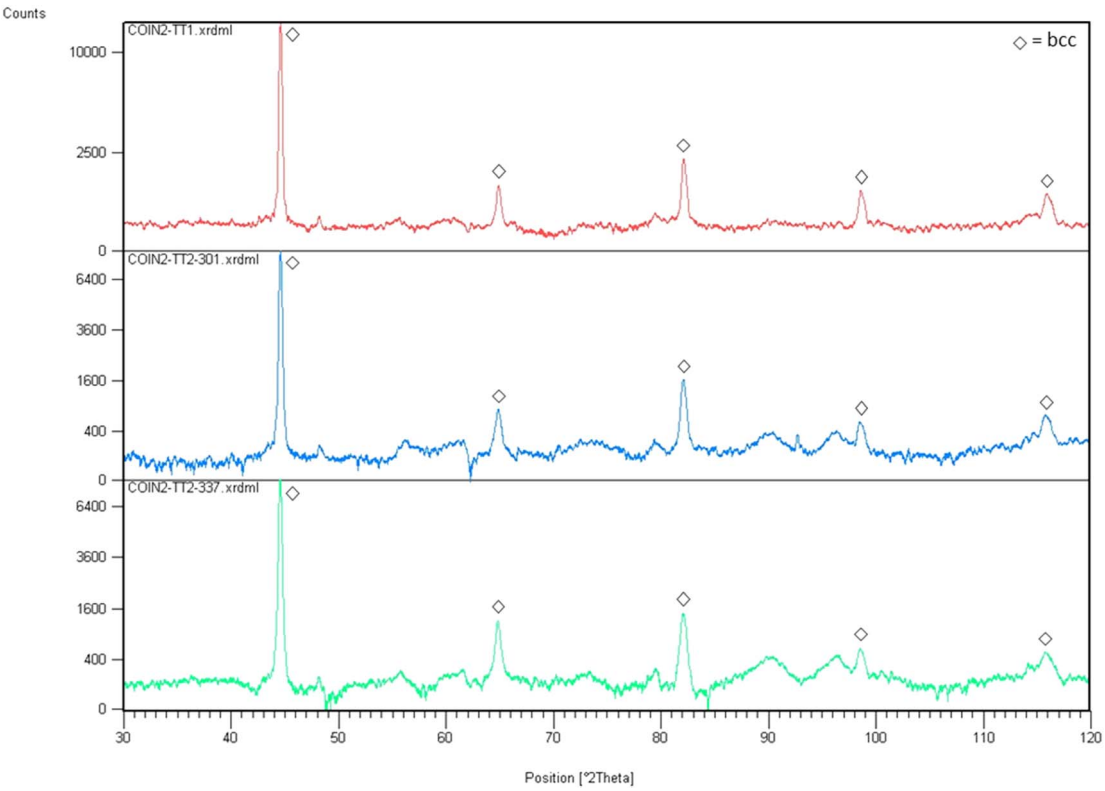

Figure 7. X-ray diffraction patterns of the dilatometry samples COIN2-TT1, COIN2-TT2–301, COIN2-TT2–337.

In order to determine the main phases present in the microstructure of the as-treated dilatometry samples, they were subjected to x-ray diffraction analysis (figure 7).

As observed in figure 7, the x-ray diffraction patterns of the three samples show predominantly phases with bcc structure, which could correspond to tempered martensite and ferrite in case of TT1, and to tempered martensite, fresh martensite [30] and ferrite [29] in case of TT2, thus confirming the results observed through dilatometry and microscopy techniques [36]. The main phase identified is martensite, as it is not possible to distinguish between ferrite, fresh martensite, and tempered martensite (the three of them can be present but

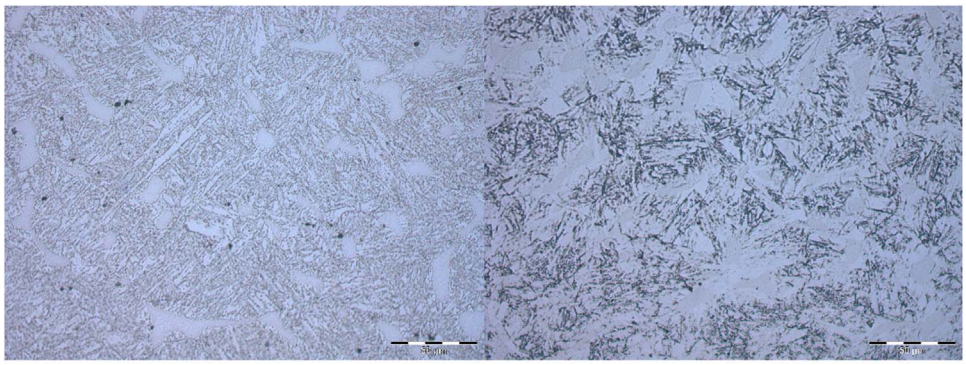

Figure 8. Microstructure of the treated cylinders (Nital etching): COIN2-TT1 (a) and COIN2-TT2–337 (b).

Table 3. Average values of the Vickers microhardness (100 g load) for the dilatometry samples of COIN2.

Steel Sample	COIN2-TT1	COIN2-TT2–301	COIN2-TT2–337
HV0,1	267 ± 4	336 ± 18	380 ± 16

only martensite/ferrite diffraction planes are identified): (110), (200), (211), (220), (310), respectively at 44,5°, 65°, 82°, 98,5°, 116°.

Table 3 shows the Vickers microhardness of the dilatometry samples COIN2-TT1, COIN2-TT2–301, COIN2-TT2–337.

As observed for COIN2 (table 3), when the microstructure is formed at a higher MT (more retained austenite), it yields more elevated microhardness. Considering these results, TT2–337 thermal treatment was designated for additional studies of COIN2, as well as TT1 for comparison.

The application of thermal treatments on lab scale samples and the corresponding characterization will help understand the microstructure evolution as well as derived mechanical behaviour given at such scale.

3.4. Thermal treatments application

Considering the characteristics shown at dilatometry scale, the heat treatments chosen to be applied on COIN2 at lab-scale were: TT1 and TT2–337. 100 mm × 45 mm cylinders were machined from the COIN2 steel grade in as-forged condition and thermally treated accordingly (TT1 and TT2–337) by muffle furnaces and a salt-bath installation. The samples after treatment were named similarly to the dilatometry samples, and were subjected to characterization at microstructural and mechanical level, as well as to the study of their creep behaviour. The characterization of the microstructure of the treated cylinders COIN2 was carried out by optical microscopy and x-ray diffraction.

3.5. Characterization

The microstructure of the treated cylinders COIN2-TT1 and COIN2-TT2–337 is shown in figure 8.

In COIN2-TT1 (figure 8(a), tempered martensite can be observed in dark colour, together with clear islands of ferrite that appear throughout the microstructure. The formation of ferrite could be due to insufficient hardenability of the steel grade for a fully martensitic microstructure.

In the case of COIN2-TT2–337 (figure 8(b)), a high percentage of austenite is retained and transformed at the end of the thermal treatment (secondary transformation) giving rise to fresh martensite that appears in clear colour [30]. There is also the possibility of ferrite formation after normalizing (as in TT1) or during tempering (from the austenite retained and stabilized, according to Tamura *et al* [29]). The high percentage of fresh martensite implies a lower concentration of martensite formed after normalizing and subsequently tempered (in dark colour). This type of martensite exhibits a more chaotic arrangement and laths of larger size in COIN2-TT2–337 rather than in COIN2-TT1.

The results observed at this scale are similar to those observed in dilatometry samples of COIN2 steel grade for the same thermal treatments.

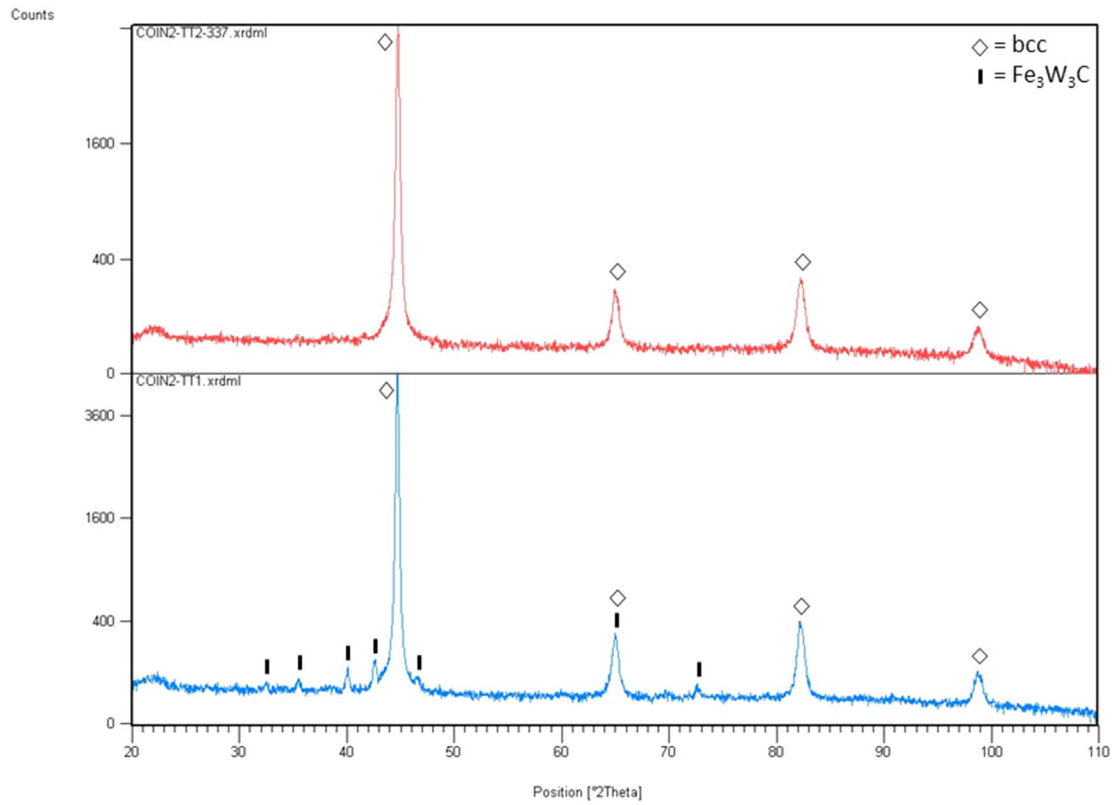

Figure 9. X-ray diffraction patterns of COIN2-TT1 (below) and COIN2-TT2–337 (above).

Table 4. Average Vickers hardness values (10 Kg load) for the treated cylinders COIN2-TT1 and COIN2-TT2–337.

Steel Sample	COIN2-TT1	COIN2-TT2–337
HV10	255 ± 3	314 ± 6

X-ray diffraction measurements were performed on the treated cylinders COIN2-TT1 and COIN2-TT2–337 in order to determine the predominant phases present in their corresponding microstructures (figure 9).

Similarly to the x-ray diffraction patterns of the dilatometry samples, the x-ray diffraction patterns of the treated cylinders COIN2-TT1 and COIN2-TT2–337 (figure 9) show the presence of phases with bcc structure, which could correspond to tempered martensite and ferrite in case of TT1, and to tempered martensite, fresh martensite [30] and ferrite [29] in case of TT2, thus supporting the results observed through microscopy technique [36]. The main phase identified is martensite, as it is not possible to distinguish between ferrite, fresh martensite, and tempered martensite (the three of them can be present but only martensite/ferrite diffraction planes are identified): (110), (200), (211), (220), (310), respectively at 44,5°, 65°, 82°, 98,5°, 116°.

In figure 9, in the case of COIN2-TT1, there are some diffraction peaks of low intensity that correspond to the Fe_3W_3C carbide (cubic, Fd-3 m, diffraction peaks at 2Theta: 32,5°, 35,5°, 40°, 42,5°, 46,5°, 65°, 72,5°). Fe_3W_3C carbide is formed near 800 °C–900 °C and can grow when subjected at higher temperatures such as 1000 °C. However, if the temperature is further increased, this type of carbides can react or dissolve, and will not be present after quenching [37]. In the case of TT2, the normalizing temperature (1150 °C) is higher than that corresponding to TT1 (1060 °C), which could be the reason why, according to the XRD diffraction measurements, Fe_3W_3C carbide can be detected in TT1, but not in the case of TT2.

The Vickers hardness and tensile properties of the treated cylinders COIN2-TT1 and COIN2-TT2–337 were measured at RT (tables 4 and 6).

In the case of COIN2, the TT2 produces higher hardness values in comparison to TT1.

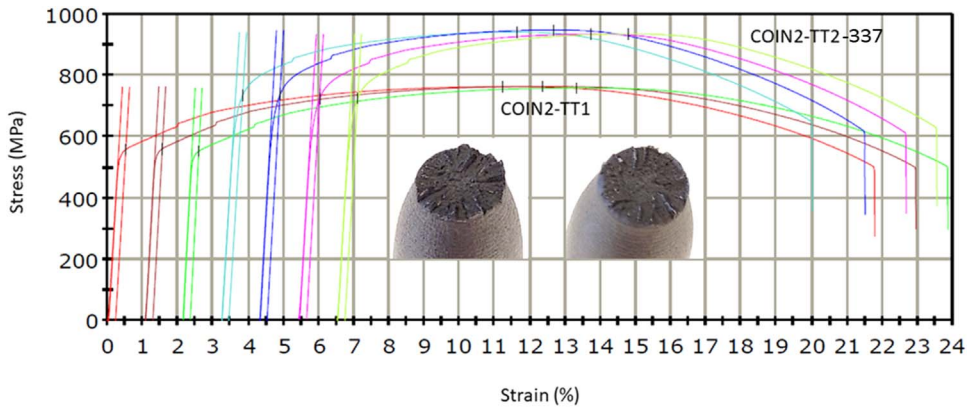

Figure 10. Stress (MPa) versus Strain (%) of COIN2-TT1 (three test samples below) and COIN2-TT2–337 (four test samples above). Fracture surfaces: COIN2-TT1 (left), COIN2-TT2–337 (right).

Table 5. Average Vickers microhardness values (50 g load) for the treated cylinders COIN2-TT1 and COIN2-TT2–337.

Steel Sample	Phase of different aspect	HV0,05	Possible correlation
COIN2-TT1	Dark	246 ± 4	Tempered martensite
	Round clear	272 ± 3	Ferrite
COIN2-TT2–337	Dark	297 ± 5	Tempered martensite
	Polygonal clear	353 ± 2	Fresh martensite
	Round clear	317 ± 1	Ferrite and carbides/carbonitrides

Table 6. Tensile properties at RT of the treated cylinders COIN2-TT1 and COIN2-TT2–337.

Steel Sample	COIN2-TT1	COIN2-TT2–337
Tensile Strength (MPa)	763 ± 2	940 ± 4
Yield Strength (MPa)	558 ± 1	730 ± 5
Elongation (%)	20 ± 4	16 ± 6
Reduction of Area (%)	64 ± 1	58 ± 2

In order to analyse in detail the different phases found in the treated cylinders COIN2-TT1 and COIN2-TT2–337, microhardness measurements were performed on each phase of the samples exhibiting different aspect (table 5).

The values obtained support the hypothesis of the microstructures described in COIN2-TT1 (tempered martensite, ferrite) and COIN2-TT2–337 (tempered martensite, fresh martensite, ferrite with carbides and/or carbonitrides).

For COIN2 steel grade (table 6 and figure 10), the tensile properties are improved with TT2 (innovative thermal treatment) in relation to TT1 (standard treatment).

Taking into account the properties of the treated cylinders of COIN2 steel grade, the innovative thermal treatment TT2 (higher austenitization temperature, higher quenching temperature after normalizing, and lower tempering temperature) originates more retained austenite (given by a more elevated martensitization temperature) and thus a higher amount of the corresponding phases after secondary transformation, which results in higher values of hardness and an improved balance of tensile properties.

The short-term creep response of the two treated cylinders COIN2-TT1 and COIN2-TT2–337 was studied at 650 °C (table 7). The stress values to apply were selected based on the creep behaviour observed in each case.

As it is shown in table 7, COIN2-TT2–337 presents a longer creep lifetime in comparison to COIN2-TT1.

The creep response of COIN2-TT1 and COIN2-TT2–337 is presented in figure 11. COIN2-TT2–337 exhibits a creep behaviour considerably enhanced in relation to COIN2-TT1. This considerable enhancement is obtained by applying TT2 (innovative thermal treatment) in comparison to TT1 (standard thermal treatment). The creep ductility of COIN2-TT2–337 is in the range of 10%–25%, which is acceptable. The fracture has ductile

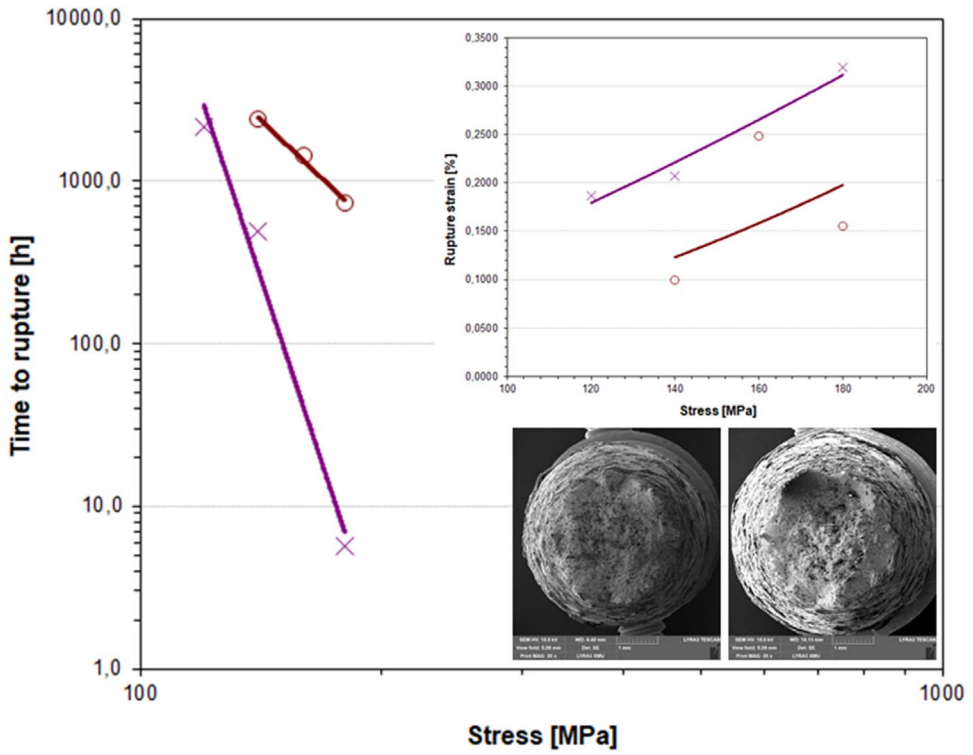

Figure 11. Time to rupture (h) versus Stress (MPa), and Rupture strain (%) versus Stress (MPa): COIN2-TT1 (X); COIN2-TT2–337 (ring). Fracture surfaces: COIN2-TT1 (left), COIN2-TT2–337 (right).

Table 7. Creep tests of COIN2-TT1 and COIN2-TT2–337.

Grade	Temperature (°C)	Thermal treatment	Time to rupture (h)	Stress (MPa)
COIN2	650	TT1	5,7	180
			488,8	140
			2172,0	120
		TT2–337	732,1	180
			1447,2	160
			2395,6	140

character with visible necking. The creep results are congruent with the hardness, tensile, and microstructural properties.

4. Discussion

These results indicate the new composition COIN2 presents a better creep response than the innovative composition COIN, which, at the same time, is more creep competitive than the standard composition P92 produced at lab scale [32]. Nevertheless, the main enhancement in terms of creep behaviour is obtained when applying the innovative thermal treatment TT2 in relation to the standard thermal treatment TT1, as indicated by the substantial improvement found for COIN2-TT2–337, COIN-TT2–342, and P92-TT2–331 steel grades in comparison to COIN2-TT1, COIN-TT1, and P92-TT1 steel grades, respectively [32].

In summary, the influence of the innovative thermal treatment on the steel properties is considerably higher than the influence of the composition innovation [32].

According to the properties observed in COIN2, the innovative thermal treatment TT2 of highest quenching temperature after normalizing and before tempering (martensitization temperature, MT) generates more retained austenite to undergo the secondary transformation into fresh martensite [30] and/or ferrite with carbides/carbonitrides [29], which originate higher values of hardness and an improved balance of tensile and

creep behaviour in relation to the application of TT1 (standard thermal treatment) or other innovative thermal treatments with MT temperatures lower than MT30.

Besides, the microprecipitates and nanoprecipitates formed exhibit high thermal stability that may support the creep behaviour detected [38, 39].

5. Conclusions

- The results of the characterization reveal a significant property improvement with the innovative thermal treatment, contributing to the production of a novel and more competitive steel grade for creep applications.
- Though, the reported research corresponds to castings and thermal treatments carried out at lab scale. For this reason, future investigations will be necessary to successfully scale up this experimental research to the industrial level.

Acknowledgments

The authors would like to thank the Institute of Physics of Materials of the Academy of Sciences of the Czech Republic of Brno, for performing the creep tests. The authors would like to thank SGIker of UPV/EHU and European funding (ERDF and ESF) for the technical and human support provided.

Data availability statement

All data that support the findings of this study are included within the article (and any supplementary files).

Funding information

This research was funded by the Basque Government under the ELKARTEK programme [KK-2019/00074].

Conflicts of interest

The authors declare there is no conflict of interest and no known competing financial interests or personal relationships that could have influenced the work reported in this paper.

ORCID iDs

Lorena M Callejo https://orcid.org/0000-0003-3293-5153

References

[1] De Sanctis M, Lovicu G, Valentini R, Dimatteo A, Ishak R, Migliaccio U, Montanari R and Pietrangeli E 2015 Microstructural features affecting tempering behavior of 16Cr-5Ni supermartensitic steel *Metall. Mater. Trans. A* **46** 1878–87
[2] Huang K-T, Chang S-H, Wu M-W and Wang C-K 2016 Effects of particle size of pre-alloy powders and vacuum sintering temperatures on the microstructure and mechanical properties of 440C stainless steel *ISIJ Int.* **56** 335–40
[3] Song P, Liu W, Zhang C, Liu L and Yang Z 2016 Reversed austenite growth behavior of a 13%Cr-5%Ni stainless steel during intercritical annealing *ISIJ Int.* **56** 148–53
[4] Matsumoto Y and Takai K 2017 Method of evaluating delayed fracture susceptibility of tempered martensitic steel showing quasi-cleavage fracture *Metall. and Mat. Trans. A* **48** 666–77
[5] Kyaw S T, Rouse J P, Lu J and Sun W 2016 Effects of surface roughness on thermo-mechanical fatigue life of a P91 power plant steel *Procedia Structural Integrity* **2** 664–72
[6] Christopher J and Choudhary B K 2018 On the onset of necking instability in tempered martensitic 9% Cr steels *Mech. Res. Commun.* **94** 114–9
[7] Benaarbia A, Xu X, Sun W, Becker A A and Jepson M A E 2018 Investigation of short-term creep deformation mechanisms in MarBN steel at elevated temperatures *Mater. Sci. Eng. A* **734** 491–505
[8] Paarmann M, Mutschler P and Sander M 2017 Numerical studies of the residual lifetime of power plant components based on experimental results at elevated temperatures *Procedia Structural Integrity* **5** 869–74
[9] El Rayes M M, El-Danaf E A and Almajid A A 2015 Characterization and correlation of mechanical, microstructural and ultrasonic properties of power plant steel *Mater. Charact.* **100** 120–34
[10] Hargadon A 2011 *The Business Of Innovating: Bringing Low-Carbon Solutions To Market; Center for Climate and Energy Solutions* (Davis. Arlington VA: University of California) (https://c2es.org/wp-content/uploads/2011/10/business-of-innovating-briging-low-carbon-solutions-to-market.pdf)

[11] Saroja S, Dasgupta A, Divakar R, Raju S, Mohandas E, Vijayalakshmi M, Bhanu K, Rao S and Raj B 2011 Development and characterization of advanced 9Cr ferritic/martensitic steels for fission and fusion reactors *J. Nucl. Mater.* **409** 131–9
[12] Pandey C, Saini N, Mahapatra M M and Kumar P 2017 Study of the fracture surface morphology of impact and tensile tested cast and forged (C&F) Grade 91 steel at room temperature for different heat treatment regimes *Eng. Fail. Anal.* **71** 131–47
[13] Pandey C, Mahapatra M M, Kumar P and Saini N 2018 Some studies on P91 steel and their weldments *J. Alloys Compd.* **743** 332–64
[14] Pandey C, Giri A and Mahapatra M M 2016 Evolution of phases in P91 steel in various heat treatment conditions and their effect on microstructure stability and mechanical properties *Mater. Sci. Eng. A* **664** 58–74
[15] Maddi L, Ballal A R, Peshwe D R, Paretkar R K, Laha K and Mathew M D 2015 Effect of tempering temperature on the stress rupture properties of Grade 92 steel *Mater. Sci. Eng. A* **639** 431–8
[16] Saini N, Pandey C and Mahapatra M M 2017 Characterization and evaluation of mechanical properties of CSEF P92 steel for varying normalizing temperature *Mater. Sci. Eng. A* **688** 250–61
[17] Tao X, Gu J and Han L 2014 Characterization of precipitates in X12CrMoWVNbN10-1-1 steel during heat treatment *J. Nucl. Mater.* **452** 557–64
[18] Vivas J, Capdevila C, Altstadt E, Houska M, Sabirov I and San-Martín D 2019 Microstructural degradation and creep fracture behavior of conventionally and thermomechanically treated 9% chromium heat resistant steel *Met. Mater. Int.* **25** 343–52
[19] Cheng Ch-D *et al* 2020 Phase transformation and mechanism on enhanced creep-life in P9 Cr–Mo heat-resistant steel *Journal of Materials Research and Technology* **9** 4617–30
[20] Vanaja J, Laha K and Mathew M D 2014 Effect of tungsten on primary creep deformation and minimum creep rate of reduced activation ferritic-martensitic steel *Metall and Mat Trans A* **45** 5076–84
[21] Chandravathi K S, Laha K, Sasmal C S, Parameswaran P, Nandagopal M, Tailor H M, Mathew M D, Jayakumar T and Kumar E R 2014 Response of phase transformation inducing heat treatments on microstructure and mechanical properties of reduced activation ferritic-martensitic steels of varying tungsten contents *Metall and Mat Trans A* **45** 4280–92
[22] Fedoseeva A, Nikitin I, Dudova N and Kaibyshev R 2021 Coarsening of laves phase and creep behaviour of a Re-containing 10% Cr-3% Co-3% W steel *Mater. Sci. Eng. A* **812** 141137
[23] Fedoseeva A, Nikitin I, Dudova N and Kaibyshev R 2020 Nucleation of W-rich carbides and laves phase in a Re-containing 10% Cr steel during creep at 650 °C *Mater. Charact.* **169** 110651
[24] Tkachev E, Belyakov A and Kaibyshev R 2020 Creep strength breakdown and microstructure in a 9%Cr steel with high B and low N contents *Mater. Sci. Eng. A* **772** 138821
[25] Tao X, Gu J and Han L 2014 Characterization of precipitates in X12CrMoWVNbN10-1-1 steel during heat treatment *J. Nucl. Mater.* **452** 557–64
[26] Xu Z, Shen Y, Shang Z, Zhang C and Huang X 2018 Precipitate phases in ferritic/martensitic steel P92 after thermomechanical treatment *J. Nucl. Mater.* **509** 355–65
[27] Kral P, Dvorak J, Sklenicka V, Masuda T, Horita Z, Kucharova K, Kvapilova M and Svobodova M 2018 Microstructure and creep behaviour of P92 steel after HPT *Mater. Sci. Eng. A* **723** 287–95
[28] Fernández P, Hoffmann J, Rieth M, Roldán M and Gómez-Herrero A 2018 TEM characterization on new 9% Cr advanced steels thermomechanical treated after tempering *J. Nucl. Mater.* **500** 1–10
[29] Tamura M, Kumagai T, Miura N, Kondo Y, Shinozuka K and Esaka H 2011 Effect of martensitizing temperature on creep strength of modified 9Cr steel *Mater. Trans.* **52** 691–8
[30] Santella M L, Swindeman R W, Reed R W and Tanzosh J M 2020 Martensite formation in 9 Cr-1 Mo steel weld metal and its effect on creep behaviour (http://citeseerx.ist.psu.edu/viewdoc/download?doi=10.1.1.526.9089&rep=rep1&type=pdf)
[31] Lu Q, Xu W and van der Zwaag S 2014 The design of a compositionally robust martensitic creep-resistant steel with an optimized combination of precipitation hardening and solid-solution strengthening for high-temperature use *Acta Mater.* **77** 310–23
[32] Callejo L M, Barbero J I, Serna-Ruiz M, Eguizabal D, Arregi B, Fernandez Martinez R, Jimbert P, Calleja-Saenz B and López A 2021 Novel creep steel developed through innovative composition and thermal treatment *Mater. High Temp.* **38** 417–25
[33] Xaubet M N, Danón C A and Ramos C P 2020 Characterization of ASTM A335 P92 Steel in Continuous Cooling Cycles (https://inis.iaea.org/search/search.aspx?orig_q=RN:46109481)
[34] Reynoso Peitsch P and Danón C A 2015 Comparative study of 9% Cr martensitic-ferritic steels using differential scanning calorimetry *Procedia Mater. Sci.* **9** 514–22
[35] DeKnijf D, Petrov R, Föjer C and Kestens L A I 2014 Effect of fresh martensite on the stability of retained austenite in quenching and partitioning steel *Mater. Sci. Eng. A* **615** 107–15
[36] Zhou T, Lu J and Hedström P 2020 Mechanical behavior of fresh and tempered martensite in a CrMoV-alloyed steel explained by microstructural evolution and strength modeling *Metallurgical and Materials Transactions A* **51A** 5077
[37] Khechba M, Hanini F and Halimi R 2011 Study of structural and mechanical properties of tungsten carbides coatings *Nature & Technology, Review* **5** 9–11
[38] https://madrimasd.org/blogs/materialesavanzados/2017/02/20/148/ (accessed on 15th of September 2020)
[39] Vivas J, Poplawsky J D, De-Castro D, San-Martín D and Capdevila C 2021 Examining the creep strengthening nanoprecipitation in novel highly reinforced heat resistant steels *Mater. Charact.* **174** 110982